Three photon decay of J/ψ from lattice QCD

Yu Meng,[1] Chuan Liu,[1,2,*] and Ke-Long Zhang[1]

[1]*School of Physics and Center for High Energy Physics, Peking University, Beijing 100871, P.R. China*
[2]*Collaborative Innovation Center of Quantum Matter, Beijing 100871, P.R. China*

(Received 17 March 2020; revised 28 May 2020; accepted 26 August 2020; published 15 September 2020)

The three-photon decay rate of J/ψ is studied using two $N_f = 2$ twisted-mass gauge ensembles with lattice spacings $a \simeq 0.085$ and 0.067 fm. Using a new method, only the correlation functions directly related to the physical decay width are computed with all polarizations of the initial and final states summed over. The final result can be obtained after a naive extrapolation to the continuum limit. To be specific, the result for such rare decay is given as $\mathcal{B}(J/\psi \to 3\gamma) = (2.13 \pm 0.14 \pm 0.29) \times 10^{-5}$, where the first error is statistical and the second is an estimate of the systematics. We also propose a method to analyze the Dalitz plot of the corresponding process based on the lattice data which can provide direct information for the relevant experiments.

DOI: 10.1103/PhysRevD.102.054506

I. INTRODUCTION

The rare decay $J/\psi \to 3\gamma$, the analogue of ortho-positronium decaying to 3γ in quantum electrodynamics [1], can provide a high-precision test for the nonperturbative quantum chromodynamics (QCD) [2]. Despite decades of effort, such a rare decay was not observed by experimentalists until 2008, when the CLEO Collaboration measured the branching fraction $\mathcal{B}(J/\psi \to 3\gamma) = (1.2 \pm 0.3 \pm 0.2) \times 10^{-5}$ for the first time [3]. With the help of much larger J/ψ samples, the BESIII Collaboration obtained the more accurate result $(11.3 \pm 1.8 \pm 2.0) \times 10^{-6}$ in 2013 [4].

On the theoretical side, using perturbative methods, the modern tool for treating the quarkonium physics is nonrelativistic QCD (NRQCD) factorization [5], in which the decay rate of $J/\psi \to 3\gamma$ is parametrized in terms of the lowest-order NRQCD J/ψ-to-vacuum matrix element with relativistic corrections $\langle v^2 \rangle_{J/\psi}$ included [6]. However, when going to higher orders, both the inconsistency between theory and experiment and the divergence puzzle arising in higher-order radiative corrections [7] indicate that NRQCD might break down for the prediction of the $J/\psi \to 3\gamma$ decay rate. Generally speaking, the perturbative calculation for the two-photon decay of charmonia is feasible because both photons can be viewed as relatively hard photons carrying roughly half of the charmonium energy. For the three-photon case, however, there is always a photon that can be very soft, thus spoiling a normal perturbative calculation. Therefore, it is fair to say that, even after three decades, the understanding of the process $J/\psi \to 3\gamma$ within NRQCD has not improved very much when compared with the situation in the early 1980s [8–10].

It is then natural to turn to genuine nonperturbative methods such as lattice QCD. Using lattice QCD, one usually evaluates the matrix element of relevant interpolating operators with correct quantum numbers between hadronic states. Although the photon itself is not an eigenstate of QCD, regarding the photon as a superposition of QCD eigenstates and adopting the electromagnetic current J^{μ}_{em} as the appropriate photon interpolating operator has been proposed already [11] and widely used in photon structure functions [12], radiative transitions [13], and two-photon decays in charmonia [14,15]. In Ref. [16] we proposed using lattice QCD as such an alternative and presented the first exploratory computation of the $J/\psi \to 3\gamma$ decay width. In this paper, we present a more detailed description of this work.

The main difference between our new method and the conventional lattice computation can be summarized as follows. In conventional lattice computations of charmonia decays involving multiple final photons, for example, in the decay of $\eta_c \to \gamma\gamma$, etc., the off-shell hadronic matrix elements such as $\mathcal{M}_{\mu\nu}$ are computed from lattice correlation functions. The same matrix elements are then parametrized using relevant form factors. Fitting these lattice data according to a prescribed functional form, one arrives at the complete form factors. Finally, the multiphoton decay width can be obtained by taking all of the final photon states on shell. In our new method, however, we focus directly on the physical decay width itself. This means that we perform the summation over polarizations of the initial

*liuchuan@pku.edu.cn

and final particles first, and the norm square of the on-shell matrix element is computed on the lattice, which we call the $\mathcal{T}$ function. The total decay width is directly related to the $\mathcal{T}$ function by a final-state phase-space integral. The advantage of this new method lies in the fact that it completely avoids the form factor decomposition step of the corresponding matrix element, which can become extremely complicated and cumbersome, especially in the case of final states with three or more photons. Moreover, these decompositions usually rely on the full Lorentz (Euclidean) invariance inherited from the continuum, which is violated on a lattice. Therefore, bypassing this decomposition is beneficial for hard photons. Another advantage is that in the case of $J/\psi \to 3\gamma$ the $\mathcal{T}$ function itself is in fact directly related to the Dalitz plot, which is also measured in experiments. In other words, we can both compute the total decay width and access the distribution of the partial decay width in the plane of two kinematic variables. One disadvantage of this method is of course that only the physical on-shell decay width can be accessed, not the complete form factors, which are also extremely useful quantities for processes involving virtual photons. Therefore, the new method and the conventional method are complementary. One possible verification of the validity of both methods lies in the process $\eta_c \to 2\gamma$. While this article was being prepared, this new method was also applied to the two-photon decay of pseudoscalar charmonium [17], where the decay width of $\eta_c \to 2\gamma$ was obtained with a result that is consistent with the experimental one within 2σ.

The rest of this paper is organized as follows. In Sec. II we give the matrix element for the three-photon decay of J/ψ and propose a new method to calculate the decay width directly without the decomposition of the relevant form factor. In Sec. III we give details of the simulations and present our main results. This section is further divided into four parts: in Sec. III A the lattice dispersion relation for J/ψ is checked; in Sec. III B the current renormalization constant is calculated; in Sec. III C the input momenta of photons are determined; in Sec. III D numerical results of the matrix element squared are presented and these results are eventually converted into the three-photon decay width of J/ψ. In Sec. IV we introduce the Dalitz analysis for the lattice simulation. This section is divided into two parts: in Sec. IV A the intermediate contribution $J/\psi \to \gamma\eta_c \to 3\gamma$ is removed, a naive continuum extrapolation is performed, and the final results are compared with the Particle Data Group value; in Sec. IV B the Dalitz plot for $J/\psi \to 3\gamma$ is predicted, which can be compared with future experiments. Finally, we conclude in Sec. V.

II. APPROACH TO THE DECAY WIDTH ON A LATTICE

A. The decay amplitude

The theoretical derivation of the decay amplitude for three photons is similar to the two-photon case. For more details, we refer interested readers to Ref. [17]. We start by expressing the decay matrix element $\langle\gamma(q_1,\lambda_1)\gamma(q_2,\lambda_2)\gamma(q_3,\lambda_3)|J/\psi(p,\lambda_0)\rangle$ in terms of the appropriate four-point function using the Lehmann-Symanzik-Zimmermann reduction formula, integrating out the photon fields perturbatively, and continuing the resulting expression to Euclidean space analytically. This process introduces the photon virtualities $Q_i^2 = |\boldsymbol{q}_i|^2 - \omega_i^2$ due to the discrete lattice momenta $\boldsymbol{q}_i = 2\pi\boldsymbol{n}_i/L$, $\boldsymbol{n}_i \in \mathbb{Z}_3$. To be specific, the energy-momentum conservation for the physical photon on the lattice cannot be simultaneously satisfied due to the discreteness of the three-momenta. Therefore, photons with virtuality are usually introduced in lattice simulations. For later convenience, we reverse the operator time ordering of the decay amplitude M and express it as

$$M(t_f,t;t',t_i) = \lim_{t_f-t\to\infty} e^3 \frac{\epsilon_\mu(q_1,\lambda_1)\epsilon_\nu(q_2,\lambda_2)\epsilon_\rho(q_3,\lambda_3)\epsilon_\alpha(p,\lambda_0)}{\frac{Z_{J/\psi}(\boldsymbol{p})}{2E_{J/\psi}(\boldsymbol{p})} e^{-E_{J/\psi}(\boldsymbol{p})(t_f-t)}} \int dt' e^{-\omega_2|t'-t|} \int dt_i e^{-\omega_1|t_i-t|}$$
$$\times \left\langle 0\left| T\left\{ \mathcal{O}^\alpha_{J/\psi}(\boldsymbol{0},t_f) \int d^3\boldsymbol{z} e^{i\boldsymbol{q}_3\cdot\boldsymbol{z}} j_\rho(\boldsymbol{z},t) \int d^3\boldsymbol{y} e^{i\boldsymbol{q}_2\cdot\boldsymbol{y}} j_\nu(\boldsymbol{y},t') \int d^3\boldsymbol{x} e^{i\boldsymbol{q}_1\cdot\boldsymbol{x}} j_\mu(\boldsymbol{x},t_i) \right\} \right| 0 \right\rangle. \quad (1)$$

Here the four polarization vectors ϵ_μ, ϵ_ν, ϵ_ρ, and ϵ_α correspond to the three final photons and the initial J/ψ particle, with the polarizations labeled as λ_1, λ_2, λ_3, and λ_0, respectively. Here the analytic continuation from Minkowski to Euclidean space works out as long as the virtualities of the photons are not too time-like to produce on-shell vector hadrons. To be specific, $Q_i^2 = |\boldsymbol{q}_i|^2 - \omega_i^2 > -M_V^2$, where M_V is the mass of the lightest vector meson. The correlation functions appearing in the above equation can be evaluated in lattice QCD in terms of quark propagators.

In this exploratory calculation, we have neglected the disconnected diagrams and only the connected diagram shown in Fig. 1 are considered. The current coupling to the first photon is fixed at time slice t_i, denoted by $j_\mu(\boldsymbol{x},t_i)$, while the other two are placed at t' and t, which are referred to as $j_\nu(\boldsymbol{y},t')$ and $j_\rho(\boldsymbol{z},t)$, respectively. The J/ψ meson is fixed at t_f as a source. The current operators in the above equation, e.g., $j_\mu(x)$, should contain all flavors of quarks weighted by their corresponding charges. However, the light quarks can only enter the question via disconnected diagrams, which are ignored in this work. For the current

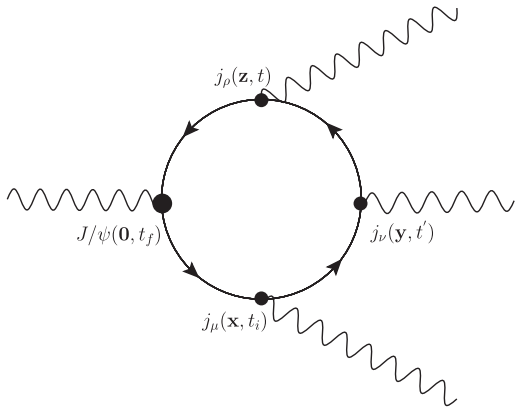

FIG. 1. Connected diagram computed for the process $J/\psi \to 3\gamma$. The J/ψ meson is fixed at time slice $t_f = T/2$, and the other time slices of the three currents j_μ, j_ν, j_ρ are denoted as t_i,t', and t, respectively. The "sequential" method has been used to calculate this four-point function. Specifically, two sequential sources are placed at time slices t_i and t, and the final contraction is performed at the sink t'.

associated with the charm quark, we utilize the local composite operator $j_\mu(x) = Z_V \bar{c}(x)\gamma_\mu c(x)$ as the current, and introduce an extra multiplicative renormalization factor Z_V. The integrals in Eq. (1) are also replaced by corresponding trapezoidal summations.

B. The decay width

For simplicity, we denote the matrix element in Eq. (1) as $M = \epsilon_\mu \epsilon_\nu \epsilon_\rho \epsilon_\alpha \mathcal{M}_{\mu\nu\rho\alpha}$ and introduce

$$\mathcal{T} \equiv \overline{|M|}^2 = \frac{1}{3}\sum_{\mu\nu\rho\sigma} |\epsilon_\mu \epsilon_\nu \epsilon_\rho \epsilon_\alpha \mathcal{M}_{\mu\nu\rho\sigma}|^2, \tag{2}$$

which will be called the $\mathcal{T}$ function in the following. The factor $1/3$ denotes the average of three polarizations of J/ψ in its rest frame. As we will see, the $\mathcal{T}$ function represents a distribution of physical partial decay widths in terms of a pair of kinematic variables. Each $\mathcal{M}_{\mu\nu\rho\alpha}$ can be computed on the lattice using the fact that M is independent of the time t, as long as $|t_f - t|$ is large enough.

In conventional lattice computations, for example, in the decay of $\eta_c \to \gamma\gamma$, etc., the hadronic matrix element (such as $\mathcal{M}_{\mu\nu\rho\alpha}$) is further decomposed into various form factors which are functions of the virtualities Q_i^2. By fitting the matrix element at different Q_i^2 with a particular functional form one arrives at the complete off-shell form factors, and finally the physical decay width can be obtained by setting all virtualities to the on-shell values, namely, $Q_i^2 = 0$. In our case, the form factor decomposition is way too complicated. The decomposition of 3γ decays of Z and positronium was worked out using perturbation theory [18,19]. However, there is no guarantee that these perturbative decompositions will also work in QCD. Therefore, we will proceed in another way. We perform the summation over polarizations of the initial and final particles first, and only the on-shell matrix element will be computed on the lattice. Due to the Ward identities of the currents, the summation over polarizations of the photons yields the Minkowski metric, e.g.,

$$\sum_{\lambda_i} (\epsilon_\mu(q_i, \lambda_i)\epsilon^*_{\mu'}(q_i, \lambda_i) \Rightarrow -g_{\mu\mu'}. \tag{3}$$

The summation over the initial polarization of J/ψ yields the same result if we use the rest frame of the particle. Therefore, we have

$$\mathcal{T} = \frac{1}{3}\sum_{\mu\nu\rho\alpha} |\mathcal{M}_{\mu\nu\rho\alpha}|^2. \tag{4}$$

In our actual simulations, we sum over all polarizations (altogether 192 possibilities) of $\mathcal{M}$.

The decay width of $J/\psi \to 3\gamma$ in J/ψ in its center-of-mass frame can be expressed as

$$\begin{aligned}\Gamma(J/\psi \to 3\gamma) &= \frac{1}{3!}\frac{1}{2m_{J/\psi}} \int \frac{d^3q_1}{(2\pi)^3 2\omega_1}\frac{d^3q_2}{(2\pi)^3 2\omega_2}\frac{d^3q_3}{(2\pi)^3 2\omega_3} \\ &\quad \times (2\pi)^4 \delta(p - q_1 - q_2 - q_3)\overline{|M|}^2 \\ &= \frac{m_{J/\psi}}{1536\pi^3}\int_0^1 dx \int_{1-x}^1 dy \mathcal{T}(x, y),\end{aligned} \tag{5}$$

where x, y are two dimensionless variables in the range [0, 1], defined as

$$x \equiv 1 - \frac{2q_2 \cdot q_3}{m^2_{J/\psi}}, \qquad y \equiv 1 - \frac{2q_1 \cdot q_2}{m^2_{J/\psi}}. \tag{6}$$

It is easily checked that they fall into the right-upper triangle of the unit square in the xy plane, i.e., satisfying $x \in [0, 1]$, $y \in [1 - x, 1]$. In the continuum, the on-shell decay patterns are normally parametrized by the so-called Dalitz plots, which can be obtained from the $\mathcal{T}$ function $\mathcal{T}(x, y)$. Due to the discreteness of the momenta on the finite lattice, it is impossible to exactly impose the on-shell condition for all particles, making the on-shell quantity $\mathcal{T}(x, y)$ not directly accessible. Instead, the on-shell conditions for the particles can be realized as follows. We first put the J/ψ particle and at least one final photon on shell, keeping the other two photons as close to on shell as possible by adjusting their three-momenta. We find that this still introduced some nonvanishing virtualities to the other photons. With these nonvanishing but small virtualities, the matrix element can be computed directly on the lattice, the norm of which we denote as $\mathcal{T}(x, y, Q_1^2, Q_2^2, Q_3^2)$. This differs from the $\mathcal{T}$ function only because of the fact that some of the photons are still not on shell. We then try to estimate the on-shell quantity, the $\mathcal{T}$ function $\mathcal{T}(x, y)$, by the following fitting formula:

TABLE I. Information for the gauge ensembles.

Ensemble	β	a (fm)	V/a^4	$a\mu_{\rm sea}$	m_π (MeV)	$N_{\rm conf}$
I	3.9	0.085	$24^3 \times 48$	0.004	315	40
II	4.05	0.067	$32^3 \times 64$	0.003	300	20

$$\mathcal{T}(x, y, Q_1^2, Q_2^2, Q_3^2) = \mathcal{T}(x, y) + \text{const} \times \sum_i Q_i^2 \quad (7)$$

where higher-order terms than $\sum_i Q_i^2$ have been drooped. We expect that such linear behavior is already good enough, which is also verified later in our paper.

Equations (1), (2), (5), and (7) constitute the central part of this paper. As pointed out already, different from the conventional method, we have intentionally avoided the amplitude parametrization for $J/\psi \to 3\gamma$, though it might have a similar structure as $Z \to 3\gamma$ [18] and the positronium-to-3γ decay [19]. Because all of the form factors introduced in the amplitude parametrizations are scalar functions of three-photon momenta, permutations of these momenta then lead to more form factors, rendering the computation of all of these form factors too costly.

III. SIMULATIONS AND RESULTS

Our lattice calculation is performed using two $N_f = 2$-flavor twisted-mass gauge field ensembles generated by the Extended Twisted Mass Collaboration with lattice spacings $a \simeq 0.067$ and 0.085 fm, respectively. The most important advantage of these configurations is the so-called automatic $\mathcal{O}(a)$ improvement for the physical quantities with a twisted-mass quark action at maximal twist [20]. In Table I we list all ensembles used in this study together with other relevant parameters. For more details about these ensembles, see Refs. [21,22]. We utilized the Osterwalder-Seiler [23] setup for the valence sector of the charm quark.

A. Mass spectrum and dispersion relation for J/ψ

The valence charm-quark mass is fixed by the physical mass of η_c with the corresponding meson operator $\hat{\mathcal{O}}_{\eta_c}(z) = \bar{c}(z)\gamma_5 c(z)$ in the physical basis. For the J/ψ meson, the operator $\hat{\mathcal{O}}_{J/\psi}(z) = \bar{c}(z)\gamma_i c(z)$ is used and the corresponding effective mass plateaus for the two ensembles are shown in the left panel of Fig. 2. The mass spectrum can be determined from these plateaus and the statistical errors are estimated using the jackknife method, with the final results summarized in Table II.

It is also crucial to verify the dispersion relation of J/ψ since the energy of J/ψ at nonzero three-momenta, namely, $E_{J/\psi}(\boldsymbol{p})$, directly enters our main result in Eq. (1). Furthermore, this verification is necessary since the dispersion relation is to be utilized to obtain the photon energies ω_i with given virtualities Q_i^2 and three-momenta $\boldsymbol{q}_i$. For this purpose, we calculate the J/ψ energies $E_{J/\psi}(\boldsymbol{p})$ at a series of three-momenta $\boldsymbol{p}$. It is found that the discrete dispersion relation

$$4\sinh^2\frac{E_{J/\psi}(\boldsymbol{p})}{2} = 4\sinh^2\frac{m_{J/\psi}}{2} + \mathcal{Z}_{\rm lat} \cdot 4\sum_i \sin^2\left(\frac{\boldsymbol{p}_i}{2}\right) \quad (8)$$

fits the energies and momenta well. In the right panel of Fig. 2, the linear behavior between $4\sinh^2\frac{E_{J/\psi}(\boldsymbol{p})}{2}$ and $4\sum_i \sin^2(\frac{\boldsymbol{p}_i}{2})$ for the two ensembles is illustrated and the slope constant $\mathcal{Z}_{\rm lat}$ is almost 1 for both ensembles, indicating that the discrete dispersion relation is well satisfied in our simulation. The small deviations of $\mathcal{Z}_{\rm lat}$ might be caused by lattice artifacts. In what follows, we

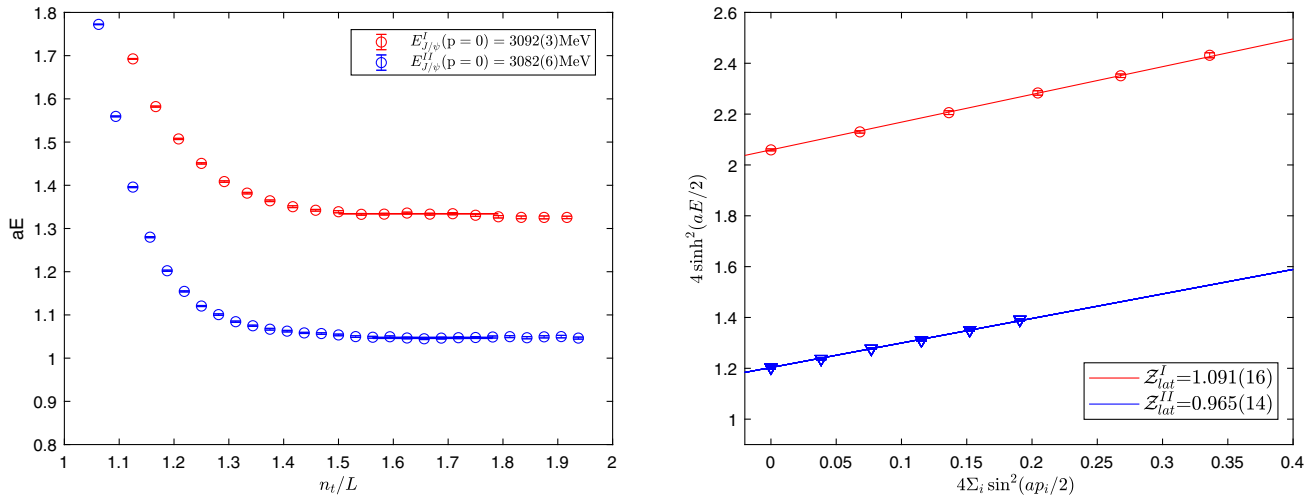

FIG. 2. The mass plateaus (left panel) and discrete dispersion relation (right panel) of J/ψ for Ens.I (red points) and Ens.II (blue points), respectively. The horizontal line segments in the left panel denote the corresponding intervals from which the energy values $E_{J/\psi}$ are extracted.

TABLE II. Numerical results for the mass, $\mathcal{Z}_{\rm lat}$, $Z_{J/\psi}$, and Z_V for J/ψ on Ens.I and Ens.II, respectively.

Ensemble	Mass [MeV]	$\mathcal{Z}_{\rm lat}$	$Z_{J/\psi}$	Z_V
I	3092(3)	1.091(16)	0.5119(45)	0.6347(26)
II	3082(6)	0.965(14)	0.2628(25)	0.6640(27)

therefore calculate the energies of the photons ω_i with virtuality Q_i^2 and momentum $\boldsymbol{q}_i$ using this discrete dispersion relation (basically, replacing $m_{J/\psi}$ by iQ_i).

The value of $Z_{J/\psi}(\boldsymbol{p})$ that appears Eq. (1) can be extracted from the two-point function

$$\Gamma_{ij}^{(2)}(\boldsymbol{p},t)\equiv\sum_{\boldsymbol{x},\boldsymbol{y}}e^{-i\boldsymbol{p}\cdot(\boldsymbol{x}-\boldsymbol{y})}\langle\mathcal{O}_i(\boldsymbol{x},t_x)\mathcal{O}_j^\dagger(\boldsymbol{y},t_y)\rangle\delta_{t,t_x-t_y}\xrightarrow[\boldsymbol{p}=0]{|t-t_f|\gg1}\frac{V\cdot|Z_{J/\psi}|^2}{E_{J/\psi}}e^{-E_{J/\psi}\frac{T}{2}}\cosh\left[E_{J/\psi}\left(\frac{T}{2}-t\right)\right],\tag{9}$$

where we have denoted $Z_{J/\psi}=Z_{J/\psi}(\boldsymbol{0})$, $E_{J/\psi}=E_{J/\psi}(\boldsymbol{0})$ for simplicity. Note that the meson J/ψ is fixed at time slice $t_f=T/2$ and a wall source is adopted in our simulations. All of these numerical results are summarized in Table II.

B. The renormalization factor Z_V

To determine the current renormalization factor Z_V, which is needed to renormalize the local current operator $j_\mu(x)=\bar{c}\gamma_\mu c(x)$, we compute the ratio of the two-point function over a three-point function [13], as given by

$$Z_V^{(\mu)}=\frac{p^\mu}{E(\mathbf{p})}\frac{\frac{1}{2}\sum_k\Gamma^{(2)}_{\psi_k\psi_k}(\mathbf{p},t_{\rm source}=T/2,t_{\rm sink}=0)}{\sum_k\Gamma^{(3)}_{\psi_k\gamma^\mu\psi_k}(\mathbf{p},t_{\rm source}=T/2,t_{\rm sink}=0,t)},\tag{10}$$

where the factor $1/2$ accounts for the equal contribution to the two-point function of the source at time slice 0 and the image of the source at time slice T. For decaying particles in the rest frame, only $\mu=0$ is needed. For simplicity, this index μ will be omitted in the following. The plateau behavior of $Z_V^{(0)}(t)$ across different time slices t then yields the value of the renormalization factor Z_V.

As an illustration, this plateau behavior is shown in Fig. 3 where the data points with errors are from our simulation and the horizontal bars indicate the intervals from which the values of Z_V are extracted. The final results of Z_V are tabulated in Table II.

C. Input parameters for three-photon decay

To compute the matrix elements in Eq. (1), it is necessary to determine all of the relevant input parameters. For a general three-body system, they include the mass, momentum, and energy of every particle. Due to the conservation

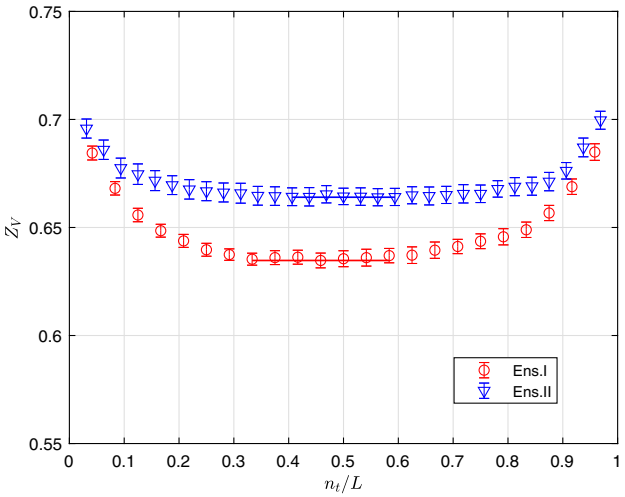

FIG. 3. The current renormalization constant $Z_V^{(\mu)}$ calculated with Eq. (10) for Ens.I and Ens.II. The horizontal colored lines denote the corresponding interval from which the values of Z_V are extracted.

of energy and momentum, there are only four independent parameters left as inputs, for example, the masses and momenta of any two particles. For a three-photon system on a lattice, we can choose the momenta $\boldsymbol{q}_i=2\pi\boldsymbol{n}_i/L$ and virtualities Q_i^2 of any two photons that meet the following requirements:

1. The corresponding (x,y) variables in Eq. (6) can cover the kinematic region as much as possible, i.e., $x\in[0,1]$, $y\in[1-x,1]$.
2. All photon virtualities satisfy $Q_i^2>-m_\rho^2$. For the ensembles in this work, the ρ-meson masses are $m_\rho^{I,II}=0.903(88)$, $1.051(50)$ GeV [15]. The ρ masses heavier than the physical ones are due to the heavier sea-quark masses on the lattice.
3. With the above conditions satisfied, we choose as few sets of photon momenta as possible.

In the case of two photons on shell, we have selected four sets of photon three-momenta for Ens.I and three sets for Ens.II as the inputs. All of the input parameters utilized in this simulation are summarized in Table III. It is easy to verify that these parameters meet the above requirements. Due to the boson exchange symmetry of the final photons, the physical amplitude $\langle J/\psi(p,\lambda_0)|\gamma(q_1,\lambda_1)\gamma(q_2,\lambda_2)\gamma(q_3,\lambda_3)\rangle$ is invariant under the photon exchange $(\boldsymbol{q}_i,\lambda_i)\leftrightarrow(\boldsymbol{q}_j,\lambda_j)$, so we finally have a total of 21 and 15 (x,y) points in the xy plane, respectively, as shown in Fig. 4.

D. On-shell $\mathcal{T}$ function and decay widths

The conventional sequential method has been adopted to calculate the four-point functions in Eq. (1). Two sequential sources are placed close to the J/ψ meson, and the contraction is performed on the furthest current, as shown in Fig. 1. After the integration (summation) of time slices t_i

TABLE III. The input parameters for the three-photon system, including the photon momenta $\boldsymbol{n}_i$, energies ω_i, and virtualities Q_i^2 which are determined in the case of two photons on shell. For the remaining off-shell photon, its virtuality satisfies $Q_2^2 > -m_\rho^2$.

Ensemble	Q_1^2	Q_3^2	$\boldsymbol{n}_1$	$\boldsymbol{n}_3$	$\boldsymbol{n}_2$	ω_1	ω_3	ω_2	x	y	Q_2^2 (GeV^2)
I	0	0	111	−1−1−2	001	0.4680	0.6525	0.2134	0.7017	0.9783	−0.1541
	0	0	111	−20 − 1	1–10	0.4680	0.5967	0.2692	0.7017	0.8946	−0.4096
	0	0	002	11 − 1	−1 − 1 − 1	0.5343	0.4680	0.3316	0.8011	0.7017	−0.6077
	0	0	002	11 − 2	−1 − 10	0.5343	0.6525	0.1471	0.8011	0.9783	−0.5690
II	0	0	210	−1 − 11	−10 − 1	0.4257	0.3320	0.2905	0.8123	0.6335	0.0932
	0	0	002	10 − 2	−100	0.3810	0.4257	0.2415	0.7269	0.8123	0.1857
	0	0	002	11 − 1	−1 − 1 − 1	0.3810	0.3320	0.3352	0.7269	0.6335	0.0187

and t', the matrix element $\mathcal{M}_{\mu\nu\rho\alpha}$, being a function of time slice t, can be obtained on the lattice. In Fig. 5, typical plateau behaviors for the four-point function $\mathcal{M}_{\mu\nu\rho\alpha}$ are shown in the case of $\mu\nu\rho\alpha = 4141$. The data points with errors are the results from the simulation and the errors are estimated using the jackknife method. Other cases are similar. The $\mathcal{T}$ function can be obtained immediately with a total 192 matrix elements $\mathcal{M}_{\mu\nu\rho\alpha}$ for each set of photon

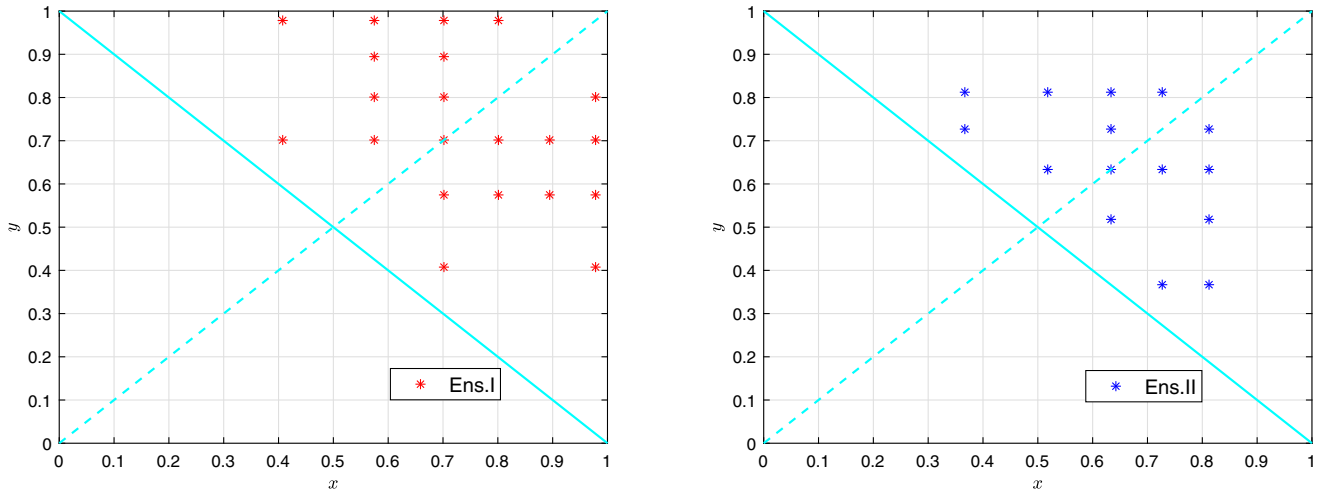

FIG. 4. Four sets of photon momenta for Ens.I (left) and three for Ens.II (right) are adopted, leading to 21 points and 15 points in the xy plane, respectively.

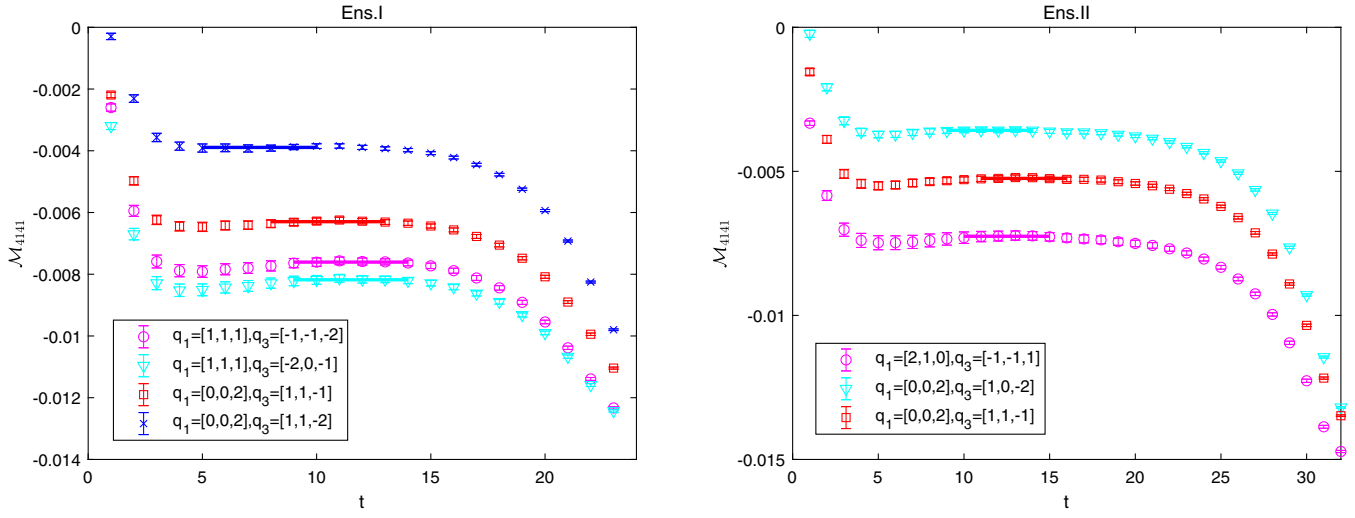

FIG. 5. The four-point function $\mathcal{M}_{\mu\nu\rho\alpha}$ as a function of t is shown in the case of $\mu\nu\rho\alpha = 4141$. Four sets of photon momenta for Ens.I (left) and three sets for Ens.II (right) are chosen to ensure that discrete data points of (x, y) can cover the integral region $x \in (0, 1)$, $y \in (1 - x, 1)$ under the condition that all virtualities are small.

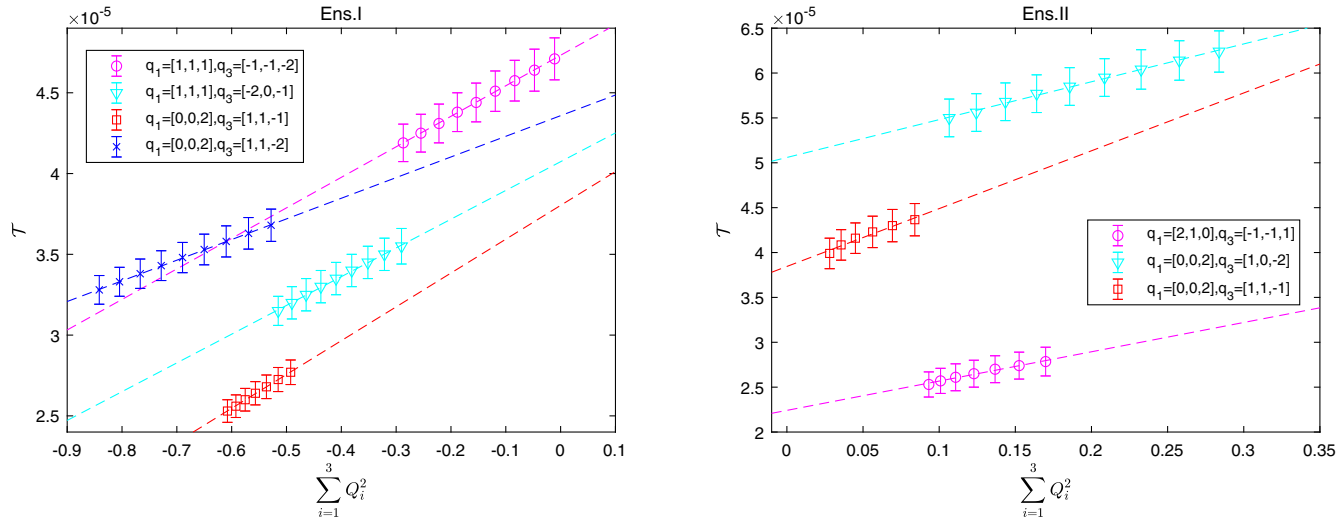

FIG. 6. On-shell $\mathcal{T}$ function for four sets of momenta for Ens.I and three sets of momenta for Ens.II are obtained by fitting Eq. (7).

momenta. However, these $\mathcal{T}$ functions are still not fully on shell. All of them still have small virtualities Q_2^2. We denote them as $\mathcal{T}(x, y, Q_1^2, Q_2^2, Q_3^2)$. To arrive at the true on-shell $\mathcal{T}$ function $\mathcal{T}(x, y, 0, 0, 0)$, we first fix $Q_1^2 = 0$, and then judiciously choose several values of Q_3^2 around the zero point $Q_3^2 = 0$. For a given set $\boldsymbol{n}_1$, $\boldsymbol{n}_2$, $\boldsymbol{n}_3$, the photon energies and virtuality Q_2^2 are then uniquely determined by the discrete dispersion relation:

$$\hat{\omega}_1^2 = 4\sum_i \sin^2(\boldsymbol{q}_{1i}/2), \tag{11}$$

$$\hat{\omega}_3^2 = 4\sum_i \sin^2(\boldsymbol{q}_{3i}/2) - \hat{Q}_3^2, \tag{12}$$

$$\omega_2 = E_{J/\psi} - \omega_1 - \omega_3, \tag{13}$$

$$\hat{Q}_2^2 = 4\sum_i \sin^2(\boldsymbol{q}_{2i}/2) - \hat{\omega}_2^2, \tag{14}$$

where $\hat{\omega}_i = \sqrt{4\sinh^2(\omega_i/2)}$ and $\hat{Q}_i^2 = 4\sinh^2(Q_i/2)$ are the lattice versions of the photon energies and virtualities, respectively. In such a way, we have obtained several off-shell $\mathcal{T}$ functions with small virtualities for each set of photon momenta. Finally, the on-shell function $\mathcal{T}(x, y)$ can be extracted by performing a correlated linear fit using Eq. (7) with the bootstrap method. In Fig. 6, we illustrate this on-shell fitting procedure for the two ensembles and they indicate that such an expansion including the linear term of $\sum_i Q_i^2$ is adequate.

To obtain the final decay width with Eq. (5), we utilize a cubic spline function to interpolate these on-shell $\mathcal{T}(x, y)$ points in the xy plane. The surfaces of these resulting interpolating functions $\mathcal{T}^{\text{int}}(x, y)$ are illustrated in Fig. 7, together with the original data points shown in red. After integrating the $\mathcal{T}$ function surface over the physical region, we finally arrive at the decay width of $J/\psi \to 3\gamma$,

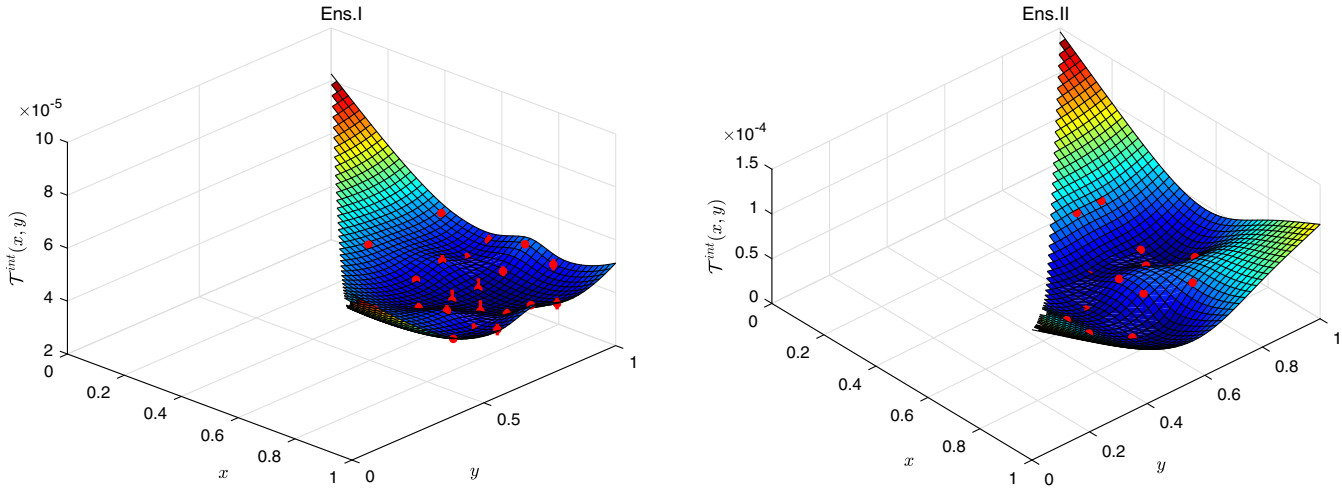

FIG. 7. The interpolated $\mathcal{T}$ function $\mathcal{T}^{\text{int}}(x, y)$ for Ens.I (left) and Ens.II (right) is shown. The red points with error bars are numerical results and the smooth surfaces are obtained from cubic spline interpolation. The physical region is limited to $x \in [0, 1]$, $y \in [1 - x, 1]$.

$$\hat{\Gamma}_I(J/\psi \to 3\gamma) = 1.530(15)\ \text{eV},$$
$$\hat{\Gamma}_{II}(J/\psi \to 3\gamma) = 1.715(47)\ \text{eV}. \quad (15)$$

Here the errors are purely statistical, arising from the current renormalization factor and the on-shell fitting process as suggested in Eq. (7).

Nevertheless, the above results are still incomplete and two key aspects have been ignored, which are outlined below:

1. First, we have computed the connected diagram as shown in Fig. 1. This diagram, in principle, can also include the physical process $J/\psi \to \gamma\eta_c \to \gamma\gamma\gamma$ as well. Therefore, in order to make a comparison with the experiments, such contributions have to be removed from our lattice data.
2. Second, due to the discreteness of the momenta on the finite lattice, the number of photon momenta utilized in the lattice simulation is very limited, making it impossible to have enough (x, y) points that cover the entire physical region, i.e., $x \in [0, 1]$, $y \in [1 - x, 1]$. For the photon momenta in this work, none of them are located in the region $x \in [0, 0.3]$, $y \in [1 - x, 1]$ and $x \in [1 - y, 1]$, $y \in [0, 0.3]$, leading to uncertainties for the interpolation results.

In the following, we will introduce the Dalitz method to analyze these difficulties.

IV. DALITZ ANALYSIS

Both experimentalists and theorists are interested in the decay widths for three-body decays. Most of the time, however, the total decay width itself is not directly measurable in experiments. Instead, the Dalitz plot, which is a distribution of the decay width in the plane of two kinematic variables, is obtained in the experiments. In the case of three-photon decay of J/ψ, this is taken to be the largest and smallest two-photon invariant mass values, denoted as $M(\gamma\gamma)_{\text{lg}}$ and $M(\gamma\gamma)_{\text{sm}}$, respectively, among three combinations for the final photons. We will call them the Dalitz variables in the following. These two Dalitz variables are in fact directly related to the kinematic variables (x, y) that we introduced above. To be more specific, we have

$$\frac{M(\gamma\gamma)_{\text{lg/sm}}}{m_{J/\psi}} = \begin{matrix}\max\\ \min\end{matrix}\left\{\sqrt{1-x}, \sqrt{1-y}, \sqrt{x+y-1}\right\}, \quad (16)$$

where the upper/lower line on the right corresponds to the case of $M(\gamma\gamma)_{\text{lg}}/M(\gamma\gamma)_{\text{sm}}$, respectively. Thus, the Dalitz plot for the three-body decay is directly related to the on-shell $\mathcal{T}$ function $\mathcal{T}(x, y)$ that we aim to compute on the lattice.

Being first-hand data obtained in the experiments, Dalitz plots play a key role for a three-body final state. As is well known, bands that appear in the Dalitz plot indicate that there is an intermediate two-body state. Thus, nonuniformity in the Dalitz plot can offer immediate information on the cross section $|\mathcal{M}|^2$.

A. Removing the $\gamma\eta_c$ contribution

For this purpose, we project the $\mathcal{T}(x, y)$ onto the xy plane and then convert it into a Dalitz plot directly. Figure 8 is the realization of this idea and also a central result of this paper. It is seen that the relation between the Dalitz variables and the pair (x, y) as indicated in Eq. (16) maps the upper right triangular region of the unit square in the (x, y) plane onto a corresponding region in the $(M(\gamma\gamma)_{\text{sm}}, M(\gamma\gamma)_{\text{lg}})$ plane in the Dalitz plot. The shape of the region in the Dalitz variables is not regular, but this is exactly what is measured in experiments; see, e.g., Fig. 1(d) in Ref. [4].

As we have obtained the interpolating functions $\mathcal{T}^{\text{int}}(x, y)$ illustrated in Fig. 7, we illustrate the mapping from the (x, y) plane to the Dalitz variables plot as suggested in Eq. (16). This is shown in Fig. 8. The contour plots of the interpolated function $\mathcal{T}^{\text{int}}(x, y)$ are shown in the left panels, while the corresponding ones in Dalitz variables are shown in the right panels.

For the two questions concerning the results of Eq. (15), we have the following comments:

(i) It is easily verified that the $\gamma\eta_c$ part corresponds to the corners of the triangle in the (x, y) plane. In the corresponding experiments, these are also the regions where the major background comes in. To remove these contributions, we need to make definite cuts, as the experimentalists did; see, e.g., Refs. [3,4]. For example, we cut these contributions by the condition $M(\gamma\gamma)_{\text{lg}} < 2.9$ GeV, which are related to the region $x \in [0, 0.1]$, $y \in [1 - x, 1]$ and $x \in [0.9, 1]$, $y \in [1 - x, 0.1]$ on the left, resulting in a deduction of 0.031 eV for Ens.I and 0.034 eV for Ens.II in the final results for $\Gamma(J/\psi \to 3\gamma)$ that are shown in Eq. (17) below.

(ii) For the physical region where no original (x, y) points are covered, we regard this contribution to the width as a systematic error. Apart from the $\gamma\eta_c$ region, the parts for this type of systematic errors are limited to the regions $x \in [0.1, 0.3]$, $y \in [1 - x, 1]$ and $x \in [1 - y, 1]$, $y \in [0.1, 0.3]$, resulting in a contribution of 0.243 eV for Ens.I and 0.274 eV for Ens.II in the final results shown in Eq. (17) below.

(iii) No obvious bands are found on the vertical region, especially for the range $M(\gamma\gamma)_{\text{sm}}(\text{GeV}) \in [0.1, 0.16]$, $[0.5, 0.6]$, $[0.9, 1]$ (GeV), which correspond to the dominant sources $\gamma\pi_0$, $\gamma\eta$, $\gamma\eta'$ in experiments [3,4]. This is understandable because such contributions are excluded in the connected diagram of J/ψ decay in Fig. 1.

Finally, we obtain the complete decay width as

$$\Gamma_I(J/\psi \to 3\gamma) = 1.499(15)(243)\ \text{eV},$$
$$\Gamma_{II}(J/\psi \to 3\gamma) = 1.681(47)(274)\ \text{eV}, \quad (17)$$

where the second errors are our estimates for the systematics, which are correlated in the two cases. The systematic

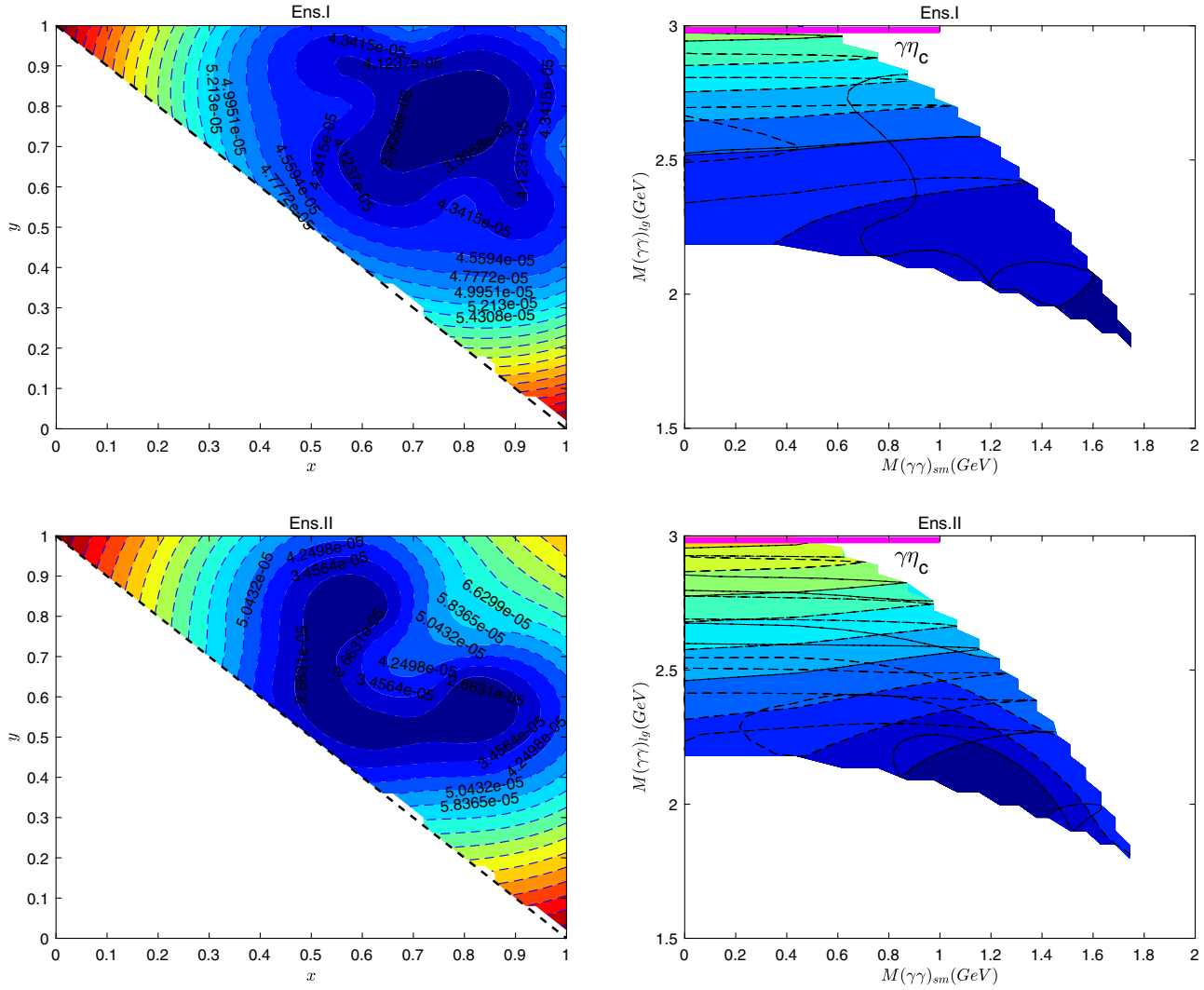

FIG. 8. The contour plots of $\mathcal{T}(x, y)$ for Ens.I and Ens.II are shown in both (x, y) variables (left two panels) and in the corresponding Dalitz variables (right two panels). The two are related to each other via Eq. (16). The black dashed lines in the left panel separate the physical region $x \in [0, 1]$, $y \in [1 - x, 1]$ and nonphysical region $x \in [0, 1]$, $y \in [0, 1 - x]$. The Dalitz plots shown in the right panel correspond to the contour plots in physical regions, while the ones in nonphysical regions fall on the vertical axis $M(\gamma\gamma)_{\mathrm{sm}}(\mathrm{GeV}) = 0$.

errors mainly come from the cubic spline interpolation process, which are obtained by estimating the integrating the results of $\mathcal{T}^{\mathrm{int}}(x, y)$ in the xy plane without the original data points, in particular, in the regions $x \in [0.1, 0.3]$, $y \in [1 - x, 1]$ and $x \in [1 - y, 1]$, $y \in [0.1, 0.3]$ for both ensembles. Note that the sizes of these two systematic errors for the two ensembles are comparable, indicating that the errors purely due to finite lattice spacing effects are not dominant at present and the major part in this systematic effect arises from the lack of data in the missing part of the phase space.

Since we only have two lattice spacing values, both with large systematic errors, we cannot make the continuum extrapolation in a controlled fashion. However, the two values at two lattice spacings indicate that this is likely within our current estimate for the systematic errors and a naive continuum extrapolation is still possible. For the study of charmonium with $N_f = 2$ configurations, one can assume $\mathcal{O}(a^2)$ errors for the lattice results for the decay widths obtained above. This allows us to connect the two results at different lattice spacings and obtain the corresponding result in the continuum limit. We call this the naive continuum extrapolation. Admittedly, this is not a well-controlled continuum extrapolation. For that purpose, one needs results for at least three or more different lattice spacings, and with more well-controlled systematic errors.

The situation of the continuum extrapolation is illustrated in Fig. 9. In this naive extrapolation, one needs to treat the statistical and systematic errors differently. The statistical errors for the two ensembles are independent of each other, while the systematic errors (as we have pointed out previously) are highly correlated. They mainly come

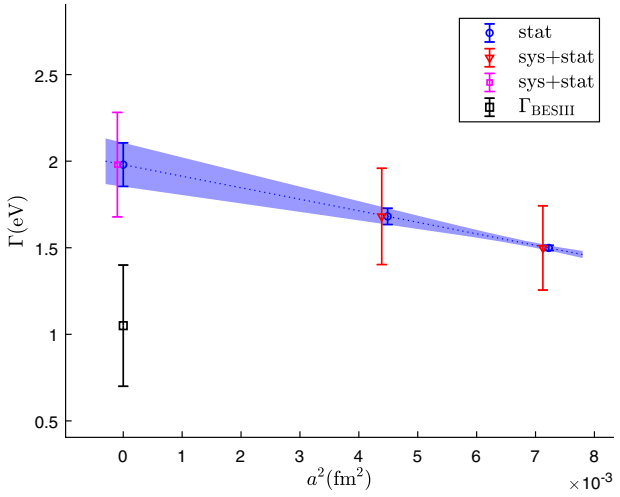

FIG. 9. A naive continuum extrapolation for the three-photon decay widths Γ_I and Γ_{II} under two different spacings $a \simeq 0.085$ and 0.067 fm, respectively. The blue points with error bars and corresponding shaded region contain only the statistical errors. The red solid triangle points contain both the statistical and systematic errors added in quadrature for each ensemble. Assuming that the majority of the systematics are highly correlated, we take the larger of the systematic errors from the two ensembles and add it in quadrature with the final statistical error in the continuum limit. This is shown as the magenta open square with the combined error at $a = 0$. The relevant points have been shifted a bit horizontally to avoid overlapping.

from the missing part of the phase space and this has little dependence on the lattice spacing. As Eq. (17) indicates, the comparable sizes of the two systematic errors also implies that the major part of this systematic error is highly correlated. Assuming this is the case, we decide to take the larger of the two systematic errors and apply it to the final continuum result. Another choice would be to add the statistical and systematic errors for each ensemble in quadrature individually and then perform the linear extrapolation. However, we believe this procedure greatly overestimates the final systematic effects. After such a naive extrapolation, the decay width for $J/\psi \to 3\gamma$ is found to be

$$\Gamma(J/\psi \to 3\gamma) = 1.98(13)(27)\ \text{eV}. \tag{18}$$

Here the first error is statistical and the second is the estimate of the systematic error, which comes from our lack of knowledge for $\mathcal{T}(x, y)$ in the regions with small x and y. Such a systematic error is inevitable for our current setup, because it is difficult to cover all points (x, y) in the physical regions. Fortunately, another scheme that we are working on will completely overcome this obstacle.

We emphasize that this result is rather preliminary due to the limited number of lattice spacings and large systematic errors. Still, our final result for the decay width of $J/\psi \to 3\gamma$ is encouraging. This the first lattice result for such a rare decay. Except for the systematic error due to the interpolation method, there are also other sources of systematic errors: finite-volume effects, a pion mass that is still far from physical value, and the contribution of disconnected diagrams. However, we think that the interpolation error is by far the most relevant error at present. Future lattice studies should aim to improve on this by utilizing more photon momenta and improved analytical methods.

If the uncertainty of the J/ψ total width is ignored, the branching fraction is given by $\mathcal{B}(J/\psi \to 3\gamma) = (2.13 \pm 0.14 \pm 0.29) \times 10^{-5}$, which is comparable with the experimental result $\mathcal{B}_{\rm exp}(J/\psi \to 3\gamma) = (1.16 \pm 0.22) \times 10^{-5}$ [24].

B. Dalitz plot for $J/\psi \to 3\gamma$

As we have clarified above, the Dalitz plot is usually the first observable obtained for three-body decays in experiments. Therefore, it is instructive to present the Dalitz plot directly, which offers a more detailed comparison of the lattice and experimental results. We therefore define a normalized $\mathcal{T}$ function distribution $\tilde{\mathcal{T}}(x, y)$ as

$$\tilde{\mathcal{T}}(x, y) = \frac{\mathcal{T}^{\rm int}(x, y)}{\int_0^1 dx \int_{1-x}^1 dy \mathcal{T}^{\rm int}(x, y)}, \tag{19}$$

which can be viewed as a probability density in the (x, y) plane. The corresponding Dalitz plot can also be generated by drawing random samples using this probability distribution.

Taking results from Ens.I as an example, in Fig. 10 we illustrate the distribution of data points drawing from the probability distribution $\tilde{\mathcal{T}}(x, y)$ defined in Eq. (19) with $N = 383$ and $N = 3314$ random samples. On the left, we show the distribution in (x, y) variables, and on the right we show the corresponding Dalitz plots. Note that the number $N = 383$ is almost the same as the number of J/ψ events observed in BESIII, whose Dalitz plot resembles that in the BESIII experiment qualitatively. The number $N = 3314$ is only an example of higher statistics, and the Dalitz plot in this case is our prediction for future experiments. Thus, we expect that BESIII would be able to observe the features with higher statistics in Fig. 10 in the future with the 1.39×10^9 J/ψ events already collected.

The importance of the Dalitz plot approach is twofold, which we briefly outline below:

1. First, it is a rather tricky process for experimentalists to extract the physical decay width of $J/\psi \to 3\gamma$, due to the lack of knowledge for such a matrix element. It is estimated that the maximum systematic uncertainty in experiments comes from the signal model used to estimate the detection efficiency, which accounts for more than 80% [4]. Therefore, the Dalitz distribution we have obtained on the lattice can act as a direct comparison with the

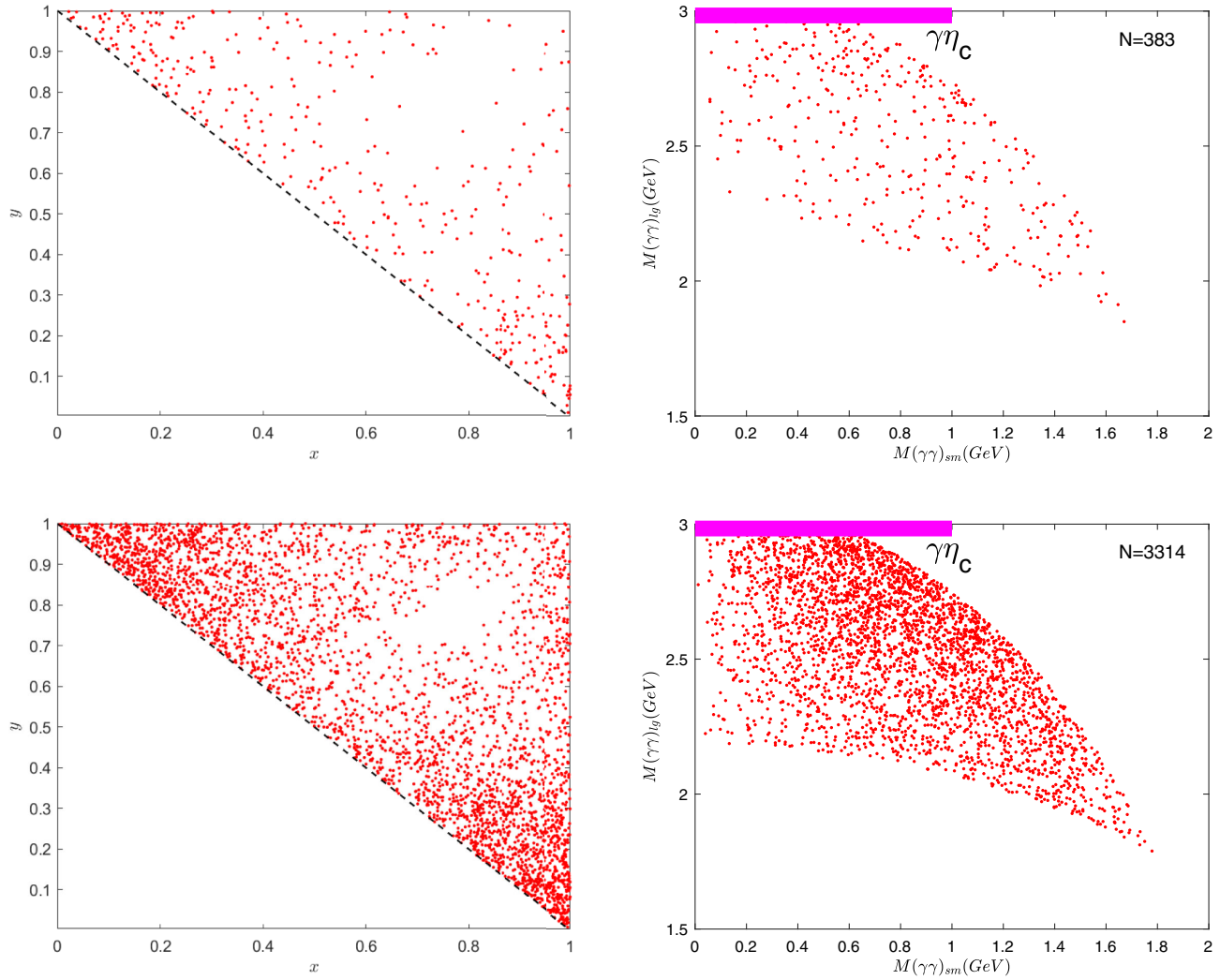

FIG. 10. The left panels are the samplings with the normalized $\mathcal{T}$ function given in Eq. (19), with $N = 383$ (top) and $N = 3314$ (bottom) samples, respectively. The right panels are the corresponding Dalitz plots. The black dashed lines on the left separate the physical region $x \in [0, 1]$, $y \in [1 - x, 1]$ and nonphysical region $x \in [0, 1]$, $y \in [0, 1 - x]$.

experiments. Carrying out the benchmark Dalitz calculations for the three-photon decay will enable experiments to implement a model-independence test for estimating the detection efficiency and, more importantly, allow both theorists and experimentalists to better understand the three-body decay process.

2. Second, with further improvements of our computing strategy, the on-shell $\mathcal{T}(x, y)$ in the continuum limit $a \to 0$ could be obtained on the lattice. Then, a parametric analytical expression for the $\mathcal{T}$ function could be set up, which could be used as the theoretical input for the matrix element of $J/\psi \to 3\gamma$. Therefore, a large number of systematic uncertainties in experiments could be avoided by adapting this expression to carry out their Monte Carlo simulation on the Dalitz plot. For more experimental details, we refer interested readers to Refs. [3,4].

V. CONCLUSIONS

To summarize, in this paper a new method has been proposed to compute hadronic decay processes with multiphoton final states. The main focus was on the process $J/\psi \to 3\gamma$, which has never been computed on the lattice before. By summing over final- and initial-state polarizations, we directly obtained the distribution of the partial decay width in the corresponding Dalitz plot, which can be compared directly with experiments. We obtained the branching fraction $\mathcal{B}(J/\psi \to 3\gamma) = (2.13 \pm 0.14 \pm 0.29) \times 10^{-5}$. The result is comparable with the two existing experimental values from CLEOc and BESIII.

One tempting advantage of this new method lies in the fact that, instead of parametrizing the relevant matrix element with form factors, we evaluate the squared matrix element which is directly related to the physical

decay width. Furthermore, we could also obtain the distribution of the partial decay width in terms of two kinematic variables, which is directly related to the Dalitz plot in the experiments. For the decay $J/\psi \to 3\gamma$, we also presented the Dalitz plot structure with more statistics, which could be verified by the BESIII Collaboration in the future.

In principle, we could also keep the information of the initial polarization of the J/ψ particle. One could also contemplate generalizing it to other hadronic decays with three particles in the final state. As a side remark, this method has been applied to processes like $\eta_c \to \gamma\gamma$ [17] and a first lattice result that is consistent with the experiments within 2σ has been obtained.

ACKNOWLEDGMENTS

The authors would like to thank Prof. Xu Feng at Peking University for helpful discussions. The authors also benefitted greatly from the discussions with the members of the CLQCD Collaboration. The numerical work was carried out on the Tianhe-1A supercomputer at Tianjin National Supercomputing Center. This work is supported in part by the National Science Foundation of China (NSFC) under Project No. 11935017 and the CAS Interdisciplinary Innovation Team project. It is also supported in part by the DFG and NSFC through funds provided to the Sino-Germen CRC 110 "Symmetries and the Emergence of Structure in QCD," DFG Grant No. TRR 110 and NSFC Grant No. 11621131001.

[1] S. G. Karshenboim, Int. J. Mod. Phys. A **19**, 3879 (2004).
[2] K. Hagiwara, C. B. Kim, and T. Yoshino, Nucl. Phys. **B177**, 461 (1981).
[3] G. S. Adams *et al.* (CLEO Collaboration), Phys. Rev. Lett. **101**, 101801 (2008).
[4] M. Ablikim *et al.* (BESIII Collaboration), Phys. Rev. D **87**, 032003 (2013).
[5] G. T. Bodwin, E. Braaten, and G. P. Lepage, Phys. Rev. D **51**, 1125 (1995); **55**, 5853(E) (1997).
[6] F. Feng, Y. Jia, and W.-L. Sang, Phys. Rev. D **87**, 051501 (2013).
[7] E. Braaten and Y.-Q. Chen, Phys. Rev. D **57**, 4236 (1998); **59**, 079901(E) (1999).
[8] P. B. Mackenzie and G. P. Lepage, Phys. Rev. Lett. **47**, 1244 (1981).
[9] W.-Y. Keung and I. J. Muzinich, Phys. Rev. D **27**, 1518 (1983).
[10] W. Kwong, P. B. Mackenzie, R. Rosenfeld, and J. L. Rosner, Phys. Rev. D **37**, 3210 (1988).
[11] X. Ji and C. Jung, Phys. Rev. Lett. **86**, 208 (2001).
[12] X. Ji and C. Jung, Phys. Rev. D **64**, 034506 (2001).
[13] J. J. Dudek, R. G. Edwards, and D. G. Richards, Phys. Rev. D **73**, 074507 (2006).
[14] J. J. Dudek and R. G. Edwards, Phys. Rev. Lett. **97**, 172001 (2006).
[15] T. Chen *et al.* (CLQCD Collaboration), Eur. Phys. J. C **76**, 358 (2016).
[16] Y. Meng, C. Liu, and K. L. Zhang, arXiv:1910.11597v3.
[17] C. Liu, Y. Meng, and K. L. Zhang, Phys. Rev. D **102**, 034502 (2020).
[18] E. W. N. Glover and A. G. Morgan, Z. Phys. C **60**, 175 (1993).
[19] G. S. Adkins, Phys. Rev. Lett. **76**, 4903 (1996).
[20] R. Frezzotti, P. A. Grassi, S. Sint, and P. Weisz (ALPHA Collaboration), J. High Energy Phys. 0108 (2001) 058, arXiv:hep-lat/0101001.
[21] P. Boucaud *et al.* (ETMC Collaboration), Phys. Lett. B **650**, 304 (2007).
[22] D. Becirevic and F. Sanfilippo, J. High Energy Phys. 01 (2013) 028.
[23] R. Frezzotti and G. Rossi, J. High Energy Phys. 10 (2004) 070.
[24] M. Tanabashi *et al.* (Particle Data Group), Phys. Rev. D **98**, 030001 (2018).